Transactions of the **14th International Conference on Structural Mechanics in Reactor Technology** (SMiRT 14), Lyon, France, August 17-22, 1997 **J03/7**

Some issues on the identification of experimental fluid-elastic forces

Bennett G.[1], Antunes J.[2], Mendes J.[2], Piteau Ph.[3]
(1) Trinity College, Dublin, Ireland
(2) Instituto Tecnologico e Nuclear (I.T.N.), Portugal
(3) CEA, France

ABSTRACT

This paper focus on least-squares methods, as applied to the experimental parameter identification in fluid-structure coupled systems. The performance of several time-domain and frequency-domain algorithms is discussed. Several important issues of the identification problem are discussed, including the optimal choice of the external excitation forces used in the identification procedure. Methods for asserting the quality of the identified results are also addressed. The discussion is supported by numerical simulations, as well as by experimental results. These are based on an experimental rig of a confined rotor, such as found in immersed pumps.

1. INTRODUCTION

The experimental identification of fluid-elastic coupling forces is a very important problem, when validating theoretical models for flow-structure interaction. Such work is seldom trivial, in particular because: (1) Being an inverse problem, system identification is often ill-conditioned; (2) The fluid-elastic forces to be identified can be much greater than the external forces used for the identification purposes; (3) The flow-coupling forces are often nonlinear; (4) The measurements are corrupted by turbulence-induced and other noises. As a consequence, fluid-elastic force identification becomes harder as the flow velocity increases, leading to quite unreliable results when the instability boundaries are approached.

This paper focus on least-squares methods, as applied to the above mentioned identification problem. Such methods are very attractive, for several reasons: (a) They are easy to implement and always converge; (b) They can be used to identify linear(ized) coupling coefficients as well as a large class of nonlinear force-terms; (c) They apply to both time-domain and frequency-domain data. Several least-squares based algorithms may be used for system identification, which lead to significant differences in performance, when difficult data is processed. This paper addresses several important issues of the identification problem, namely:

- The external excitation forces used for identification, and how results depend on the force time-histories;
- The time-domain and frequency-domain implementations of least-squares algorithms, and their merits;

- The ordinary-least-squares and total-least-squares identification methods, and their respective performances;
- How to assert the quality of the identified results.

The discussion is supported by extensive numerical simulations, as well as by experimental results. The system under concern is a rotor immersed in a dense fluid (such as water or sodium), subject to moderate confinement (typically, the reduced annular fluid gap is $\delta=H/R\approx 0.1$). The prediction of the dynamic behaviour of such system is very important, in connection with the design of fast-breather reactor pumps.

Identification of the linearized fluid-elastic forces is based on the theoretical model previously developed by Axisa & Antunes (1992), Grunenwald (1994) and Antunes et al. (1996). Here, the theoretical flow-coupling coefficients are compared with those stemming from the identification procedures. The suitability of several excitation and identification techniques is based on numerical simulations of the rotor system, for both plane and orbital motions. In these numerical simulations, the dynamic equations obtained by Axisa & Antunes (1992) are time-step integrated, the system responses being polluted with several levels of noise contamination. The theoretical flow-coupling coefficients are then compared with the identified results. On the other hand, a limited number of experimental identifications has been achieved, in our ongoing test programme.

2. SYSTEM IDENTIFICATION METHODS

2.1 *Time-domain techniques*

a) Identification based on the correlation matrix

The first method presented may be seen as a direct time-domain extension of the Rice & Fitzpatrick (1988) basic algorithm, where the auto and cross-spectrums used by these authors are now replaced by auto and cross-correlation coefficients. Let us assume a two-dimensional linear system with responses $x(t)$ and $y(t)$ to external forces $F_x(t)$ and $F_y(t)$:

$$\begin{bmatrix} M_{xx} & M_{xy} \\ M_{yx} & M_{yy} \end{bmatrix} \begin{Bmatrix} \ddot{x} \\ \ddot{y} \end{Bmatrix} + \begin{bmatrix} C_{xx} & C_{xy} \\ C_{yx} & C_{yy} \end{bmatrix} \begin{Bmatrix} \dot{x} \\ \dot{y} \end{Bmatrix} + \begin{bmatrix} K_{xx} & K_{xy} \\ K_{yx} & K_{yy} \end{bmatrix} \begin{Bmatrix} x \\ y \end{Bmatrix} = \begin{Bmatrix} F_x(t) \\ F_y(t) \end{Bmatrix} \tag{1}$$

From the input signals a matrix equation is constructed with the auto and cross-correlation coefficients. On the other hand, from the input and each output signals, vectors o cross-correlation coefficients are formed. Hence, the following matrix equations are obtained:

$$\begin{bmatrix} C_{\ddot{x}\ddot{x}} & C_{\ddot{x}\ddot{y}} & \cdots & C_{\ddot{x}\dot{y}} \\ C_{\ddot{y}\ddot{x}} & C_{\ddot{y}\ddot{y}} & \cdots & C_{\ddot{y}\dot{y}} \\ \vdots & \vdots & \ddots & \vdots \\ C_{y\ddot{x}} & C_{y\ddot{y}} & \cdots & C_{yy} \end{bmatrix} \begin{bmatrix} \begin{Bmatrix} M_{xx} \\ M_{xy} \\ C_{xx} \\ C_{xy} \\ K_{xx} \\ K_{xy} \end{Bmatrix}, \begin{Bmatrix} M_{yx} \\ M_{yy} \\ C_{yx} \\ C_{yy} \\ K_{yx} \\ K_{yy} \end{Bmatrix} \end{bmatrix} = \begin{bmatrix} \begin{Bmatrix} C_{\ddot{x}F_x} \\ C_{\ddot{y}F_x} \\ \vdots \\ C_{yF_x} \end{Bmatrix}, \begin{Bmatrix} C_{\ddot{x}F_y} \\ C_{\ddot{y}F_y} \\ \vdots \\ C_{yF_y} \end{Bmatrix} \end{bmatrix} \tag{2}$$

which can be represented by,

$$[\mathbf{C}]\{\mathbf{A}\} = \{\mathbf{D}\} \tag{3}$$

and the coefficients to identify are given as:

$$\{\mathbf{A}\} = [\mathbf{C}]^{-1}\{\mathbf{D}\} \tag{4}$$

b) Identification based on ordinary-least-squares

The following matrix equations can be formed directly from the sampled data signals:

$$\left[\begin{Bmatrix}\ddot{x}(t_1)\\ \ddot{x}(t_2)\\ \vdots\\ \ddot{x}(t_n)\end{Bmatrix}\begin{Bmatrix}\ddot{y}(t_1)\\ \ddot{y}(t_2)\\ \vdots\\ \ddot{y}(t_n)\end{Bmatrix}\begin{Bmatrix}\dot{x}(t_1)\\ \dot{x}(t_2)\\ \vdots\\ \dot{x}(t_n)\end{Bmatrix}\begin{Bmatrix}\dot{y}(t_1)\\ \dot{y}(t_2)\\ \vdots\\ \dot{y}(t_n)\end{Bmatrix}\begin{Bmatrix}x(t_1)\\ x(t_2)\\ \vdots\\ x(t_n)\end{Bmatrix}\begin{Bmatrix}y(t_1)\\ y(t_2)\\ \vdots\\ y(t_n)\end{Bmatrix}\right]\left[\begin{Bmatrix}M_{xx}\\ M_{xy}\\ C_{xx}\\ C_{xy}\\ K_{xx}\\ K_{xy}\end{Bmatrix}\begin{Bmatrix}M_{yx}\\ M_{yy}\\ C_{yx}\\ C_{yy}\\ K_{yx}\\ K_{yy}\end{Bmatrix}\right]=\left[\begin{Bmatrix}F_x(t_1)\\ F_x(t_2)\\ \vdots\\ F_x(t_n)\end{Bmatrix}\begin{Bmatrix}F_y(t_1)\\ F_y(t_2)\\ \vdots\\ F_y(t_n)\end{Bmatrix}\right] \tag{5}$$

and the coefficients to identify are given as

$$[\tilde{\mathbf{C}}]\{\mathbf{A}\}=\{\tilde{\mathbf{D}}\} \qquad \rightarrow \qquad \{\mathbf{A}\}=[\tilde{\mathbf{C}}]^{+}\{\tilde{\mathbf{D}}\} \tag{6,7}$$

where

$$[\tilde{\mathbf{C}}]^{+}=\left[[\tilde{\mathbf{C}}]^{T}[\tilde{\mathbf{C}}]\right]^{-1}[\tilde{\mathbf{C}}]^{T} \tag{8}$$

is the Moore-Penrose pseudo-inverse of the input correlation coefficient matrix. All matrix inversions and pseudo-inversions such as (8) will be always performed using a SVD algorithm with truncation of the ill-conditioning singular values. It can be easily demonstrated (Therrien, 1992) that formulation (6-8) is equivalent to the ordinary-least-squares fit of model (1) to the experimental data. Therefore, coefficients $\{\mathbf{A}\}$ lead to a minimum L_2 norm of the error between the theoretical formulation and the noisy signals.

2.2 *Frequency-domain techniques*

By Fourier transforming equation (1), a similar equation to (2) can be written in the frequency domain. Then, auto and cross-correlation coefficients are replaced by auto and cross-spectra of the measurements. For each frequency f, one obtains:

$$\begin{bmatrix}S_{\ddot{x}\ddot{x}}(f) & S_{\ddot{x}\ddot{y}}(f) & \cdots & S_{\ddot{x}y}(f)\\ S_{\ddot{y}\ddot{x}}(f) & S_{\ddot{y}\ddot{y}}(f) & \cdots & S_{\ddot{y}y}(f)\\ \vdots & \vdots & \ddots & \vdots\\ S_{y\ddot{x}}(f) & S_{y\ddot{y}}(f) & \cdots & S_{yy}(f)\end{bmatrix}\left[\begin{Bmatrix}M_{xx}\\ M_{xy}\\ C_{xx}\\ C_{xy}\\ K_{xx}\\ K_{xy}\end{Bmatrix}\begin{Bmatrix}M_{yx}\\ M_{yy}\\ C_{yx}\\ C_{yy}\\ K_{yx}\\ K_{yy}\end{Bmatrix}\right]=\left[\begin{Bmatrix}S_{\ddot{x}F_x}(f)\\ S_{\ddot{y}F_x}(f)\\ \vdots\\ S_{yF_x}(f)\end{Bmatrix}\begin{Bmatrix}S_{\ddot{x}F_y}(f)\\ S_{\ddot{y}F_y}(f)\\ \vdots\\ S_{yF_y}(f)\end{Bmatrix}\right] \tag{9}$$

This formulation is particularly useful if the system coefficients are frequency-dependent.

2.3 *Further refinements*

Total-least-squares is a powerful extension of the classical least squares. It is ideally suited for situations in which all data are corrupted by noise, which is almost always the case in engineering applications. The idea is to process *all* data signals (inputs and outputs) using an augmented data matrix, in such a way that some error norm is minimized. Hence, in ordinary-least-squares, we seek to minimize the norm L_2 of the error vector Σ in the over-determined system

$$[\tilde{\mathbf{C}}]\{\mathbf{A}\}=\{\tilde{\mathbf{D}}\}-\{\Sigma\} \tag{10}$$

where the implicit assumption is that the error is associated with the vector $\{\tilde{\mathbf{D}}\}$. In total-least-squares, an error is associated with both $[\tilde{\mathbf{C}}]$ and $\{\tilde{\mathbf{D}}\}$, which is reasonable, since they all represent measured (noisy) data. Therefore, we write

$$[\tilde{\mathbf{C}} - \Delta]\{\mathbf{A}\} = \{\tilde{\mathbf{D}}\} - \{\Sigma\} \tag{11}$$

where $[\Delta]$ is the error matrix associated with the inputs. Equation (11) is reformulated as

$$[\overline{\mathbf{C}} - \overline{\Delta}]\begin{Bmatrix}\mathbf{A}\\ -\mathbf{1}\end{Bmatrix} = \{\mathbf{0}\} \quad \text{where} \quad [\overline{\mathbf{C}}] = [[\tilde{\mathbf{C}}], \{\tilde{\mathbf{D}}\}] \quad \text{and} \quad [\overline{\Delta}] = [[\Delta], \{\Sigma\}] \tag{12}$$

hence we have a completely symmetrical weighing of all measurement errors. The solution of this problem involves the SVD of the composite data matrix $[\overline{\mathbf{C}}]$ (see Van Huffel & Zha, 1993).

3. THEORETICAL RESULTS

3.1 *Vibrations of immersed rotors*

A detailed formulation for the flow equations has been presented elsewhere (Grunenwald, 1994; Antunes et al., 1997) and will not be repeated here. Under the so-called "bulk-flow" assumption, one obtains the continuity and momentum (in the tangential direction) equations for incompressible flow

$$\frac{\partial h}{\partial t} + \frac{1}{R}\frac{\partial}{\partial \theta}(hu) = 0 \quad ; \quad \rho\left[\frac{\partial}{\partial t}(hu) + \frac{1}{R}\frac{\partial}{\partial \theta}(hu^2)\right] + \tau_r + \tau_s + \frac{h}{R}\frac{\partial p}{\partial \theta} = 0 \tag{13,14}$$

where R is the shaft radius, $h(\theta,t)$ is the annular gap depth, $u(\theta,t)$ is the gap-averaged tangential flow velocity, ρ is the volumic mass of the fluid and $p(\theta,t)$ is the gap-averaged pressure. The shear stresses at the rotor and stator walls are given by

$$\tau_r = -\frac{1}{2}\rho(\Omega R - u)^2 f_r \quad ; \quad \tau_s = \frac{1}{2}\rho u^2 f_s \tag{15,16}$$

where f_r and f_s are empirical friction coefficients, which depend on the flow Reynolds number and on wall rugosity. Among several empirical correlations, those suggested by Wend (1933) and Hirs (1973) are formulated as $f = a\,(Re)^b$, where coefficients a and b are obtained from experiments. We consider a generic planar motion $\{x(t), y(t)\}$ leading to the flow gap

$$h(\theta,t) \cong H - x(t)\cos\theta - y(t)\sin\theta \tag{17}$$

and are interested in the resulting dynamic flow forces, computed by integrating the pressure

$$F_x^{flow}(t) = -L R \int_{-\pi}^{\pi} p(\theta,t)\cos\theta\, d\theta \quad ; \quad F_y^{flow}(t) = -L R \int_{-\pi}^{\pi} p(\theta,t)\sin\theta\, d\theta \tag{18,19}$$

where L is the immersed length of the rotor. From linearized equations (13-17), the flow velocity $u(\theta,t)$ and pressure fields $p(\theta,t)$ are computed. Then integrations (18,19), together with the structure dynamics, lead to a coupled rotor-flow formulation in the form (1) — see the above mentioned references for details and results. From the autonomous version of equation (1), eigenvalues and eigenvectors of the linearized coupled system may be computed, as a function of the rotor spinning velocity. Also, for each configuration, the stability boundaries may be computed.

3.2 *Numerical simulations*

For a centered rotor-flow configuration, the basic system of two second-order differential equations (1) is transformed in the equivalent system of four first-order equations. In accordance with the theoretical flow model (Antunes et al., 1997) we obtain:

$$\begin{Bmatrix} \dot{Z}_1 \\ \dot{Z}_2 \\ \dot{Z}_3 \\ \dot{Z}_4 \end{Bmatrix} = \begin{bmatrix} 0 & 1 & 0 & 0 \\ -\dfrac{M_r\omega_r^2 - \dfrac{\Omega^2 M_a}{4}}{M_T} & -\dfrac{2M_r\omega_r\varsigma_r}{M_T} - \dfrac{\Omega M_a f}{\delta} & -\dfrac{\Omega^2 M_a f}{2\delta} & -\dfrac{\Omega M_a}{M_T} \\ 0 & 0 & 0 & 1 \\ \dfrac{\Omega^2 M_a f}{2\delta} & \dfrac{\Omega M_a}{M_T} & -\dfrac{M_r\omega_r^2 - \dfrac{\Omega^2 M_a}{4}}{M_T} & -\dfrac{2M_r\omega_r\varsigma_r}{M_T} - \dfrac{\Omega M_a f}{\delta} \end{bmatrix} \begin{Bmatrix} Z_1 \\ Z_2 \\ Z_3 \\ Z_4 \end{Bmatrix} + \begin{Bmatrix} 0 \\ \dfrac{1}{M_T}F_x(t) \\ 0 \\ \dfrac{1}{M_T}F_y(t) \end{Bmatrix} \qquad (20)$$

Here $M_T = M_{rotor} + M_{flow}$ where M_{flow} is the fluid added mass and $M_{xy} = M_{yx} = 0$. Also, the following state-space variables apply:

$$Z_1 = x(t) \;\; ; \;\; Z_2 = \dot{x}(t) \;\; ; \;\; Z_3 = y(t) \;\; ; \;\; Z_4 = \dot{y}(t)$$

Equations (20) were simultaneously solved using an explicit fifth order integration algorithm of the Runge-Kutta type, with an automatic error-controlled time-step. External excitation was produced by two uncorrelated random forces in the frequency range 0~15 Hz. The integration time-step was $\Delta t = 10^{-3}$ s and 50 seconds of the system responses were simulated, for each spinning velocity Ω=0~1000 rpm. Numerical simulations were based on the configuration shown in Table 1, which follows closely the experimental setup. A typical flow friction coefficient of f=0.01 was used when computing the dissipative terms related to the rotor velocity.

TABLE 1
PARAMETERS OF THE NUMERICAL SIMULATIONS

Structure		*Flow*	
$M_{xx}=M_{yy}$=10 Kg	; $M_{xy}=M_{yx}=0$	$M_{xx}=M_{yy}=M_{flow}$=50 Kg	; $M_{xy}=M_{yx}=0$
$C_{xx}=C_{yy}$=12.57 Ns/m	; $C_{xy}=C_{yx}=0$	$C_{xx}=C_{yy}=\Omega M_{flow} f/\delta$	; $C_{xy}=-C_{yx}=-\Omega M_{flow}$
$K_{xx}=K_{yy}$=3.95 10^4 N/m	; $K_{xy}=K_{yx}=0$	$K_{xx}=K_{yy}=-\Omega^2 M_{flow}/4$	; $K_{xy}=-K_{yx}=\Omega^2 M_{flow} f/(2\delta)$

Results were based on the average of ten identifications, each one performed on a 5 s block data. In all cases, the exact signals were polluted with additive random noises with given root-mean-square levels.

3.3 *Identification results*

Due to lack of space we only present the results from time-domain identifications, which usually produced more reliable results. However, frequency-domain methods are most useful when the system coefficients are frequency-dependent and also proved fruitful for insight. Figure 1 presents the identified flow coefficients and eigenvalues (frequencies and damping values) from the time-domain test-case simulated data, for no noise contamination. These results are exact and all identification methods performed very well. However, significant differences arise when noisy data is processed. Figure 2 applies to both the correlation and ordinary least-squares identification methods, which produced identical results. At 20 % noise contamination a noticeable degradation of the identified flow coefficients is clear. In this figure, the average coefficients (from 10 data blocks) are presented (crosses connected by lines) as well as the corresponding "dispersion bands" (solid lines). Figure 3, obtained using the total least-squares algorithm, shows a clear improvement of the results. The inertia terms are well identified by the total-least-squares, even at high velocities, while the other methods severely underestimate these coefficients. The gyroscopic and stiffness terms were also better identified by the total-least-squares method.

Results were obtained from signals which were previously normalized to unit rms magnitude, in order to insure that all terms were equally weigthed by the identification procedures. Also, data filtering was found usefull to extract the most meaningful data range. Identification results consistently deteriorated at high flow velocities, when fluidelastic forces are much higher than the external force imposed for the system identification. The dispersion of the identified results, as given by the "root-mean-squares bands" from several identifications, was found to be the best confidence indicator of the results quality. Indeed, good results are stable whereas unreliable results display a significant dispersion. The correlation coefficients (global or parcial) between data are often inconclusive, when the relative importance of identified terms is accessed. This aspect certainly needs further research efforts.

4. EXPERIMENTAL RESULTS

4.1 *Test rig*

The experimental setup is described in detail by Grunenwald et al. (1996). It consists on a cylindrical shaft with length L=250 mm and radius R=43.5 mm, which rotates inside a rigid outer shell with radial gap H=6.7 mm (e.g., δ=0.15). The shaft is mounted using a pair of conical bearings, assembled in a rigid support plate, maintained by four identical flexible steel struts. The translation stiffness provided by the struts was such that $K_{sx}=K_{sy}=1.6\ 10^4$ N/m. The measured structural mass was M_s=7.0 Kg and the theoretical added mass was M_{flow}=12.5 Kg. Steady rotation was provided by an electric motor, with precise velocity control, using a double cardan joint for torque transmission. A large-gap labyrinth, on the upper part of the rotor, was used to prevent surface effects and flow ventilation at higher velocities. All experiments concern a centered shaft configuration. Excitation was provided by a pair of orthogonal shakers driven by uncorrelated random or sinusoidal sweep signals. Rotor vibrations and whirling motions were sensed using two orthogonal non-contacting eddy-current displacement sensors and two accelerometers. The excitation forces were measured using two piezo-electric transducers. All signals were filtered, conditioned, pre-amplified, digitized and recorded before analysis, which was performed using a computer-based signal processing system.

4.2 *Rotor dynamics*

Figure 4 shows the theoretical and identified modal frequencies and damping values of the coupled system, as a function of the rotor spinning velocity Ω. The eigenvalue of the nonrotating system splits into a forward and a backward modes until about 650 rpm. Then the backward mode changes into a second forward mode. For sufficiently high velocities (Ω >1300 rpm), the system displays a flutter instability. All these motion regimes are thoroughly discussed by Antunes et al. (1996) and Grunenwald et al. (1996). More important, Figure 4 shows that the identified modes agree fairly well with the theoretical model, at least in the range $0<\Omega<1000$ rpm. Here, uncorrelated F_x and F_y sinusoidal sweeps were used for excitation of the system. These results are of the same quality as those obtained using random forces. However it was found that correlated *backward orbiting* sweep forces may produce better identifications at higher velocities, which is a relevant result.

4.3 *Identification results*

The results presented in Figure 5 were obtained using the total least-squares identification method in the time-domain. Here the 12 coupling coefficients by the flow are shown as a function of the rotor speed. One may notice that most of the theoretical model predictions from the linearized model are respected, as far as the qualitative behavior is concerned. However, several significant discrepancies may be noticed. For instance, the added mass coefficients M_{xx} and M_{yy} decrease at higher spinning velocities, whereas theory predicts a constant value. On the other hand, the identified cross-coupling terms M_{xy} and M_{yx} increase significantly with Ω, when theory predicts null values. The identified damping terms C_{xx} and C_{yy} increase with the spinning velocity, as predicted, but at higher values. The gyroscopic terms C_{xy} and C_{yx} closely follow the theoretical model, until an unexpected saturation arises at about 700 rpm. Similarly, the negative flow-coupling stiffness coefficients K_{xx} and K_{yy} are in close agreement with the quadratic law predicted by theory, but a perturbation is displayed at 700 rpm. The identified circulatory coefficients K_{xy} and K_{yx} also follow the theoretical predictions, which are however of lower magnitude. These discrepancies may be due to identification difficulties, but also to some inadequacies of the theoretical model — for instance, significant nonlinear effects at higher velocities. These problems are being addressed in our current work.

5. CONCLUSIONS

The identification of fluidelastic forces in flow-structure coupled systems is still a difficult problem. However, if the noise contamination is moderate and the system is operating well below the instability boundaries, least-squares based techniques may provide feasible identifications. Furthermore, from the numerical simulations and experimental results obtained, the following conclusions may be drawn:

- Time-domain identification approaches usually perform better, for a given amount of data, however, frequency-domain identification may help understanding the results;
- The total least-squares algorithm definitely leads to improved results, under noise contamination and when approaching instability (at least for the problem in hand);
- Among several wide-band (random and deterministic) external forces used to drive the system, better results can be obtained with backward orbital excitations.
- At the present time, the best way to assert the quality of the identified results is by observing the dispersion of several identifications. Good results are stable and unreliable results display a significant dispersion.

Further work is definitely needed in order to insure robust identifications, in particular when dealing with almost-unstable systems and/or under severe turbulence contamination. These issues are obviously emphasized if nonlinear identification is addressed.

REFERENCES

1. Antunes, J., Axisa, F., Grunenwald, T. 1996. Vibrations of Rotors Immersed in Eccentric Annular Flow: Part 1 - Theory, *Journal of Fluids and Structures,* 10: 893-918.

2. Axisa, F., Antunes, J. 1992. Flexural Vibrations of Rotors Immersed in Dense Fluids: Part 1 - Theory, *Journal of Fluids and Structures,* 6: 3-21.

3. Grunenwald, T. 1994. *Comportement Vibratoire d'Arbres de Machines Tournantes dans un Espace Annulaire de Fluide de Confinement Modéré*, Doctoral Thesis, Paris University, September 1994.
4. Grunenwald, T., Axisa, F., Bennett, G., Antunes, J. 1996. Vibrations of Rotors Immersed in Eccentric Annular Flow: Part 2 - Experiments, *Journal of Fluids and Structures*, 10: 919-944.
5. Hirs G. G. 1973. A Bulk-Flow Theory for Turbulence in Lubricant Films, *ASME Journal of Lubrication Technology*, 95: 137-146.
6. Rice, H., Fitzpatrick, J. 1988. A generalized technique for spectral analysis of nonlinear systems, *Mechanical Systems and Signal Processing*, 2: 195-207.
7. Therrien, C. W. 1992. *Discrete Random Signals and Statistical Signal Processing*, London: Prentice-Hall International Editions.
8. Van Huffel S., Zha H. 1993. The Total-Least-Squares Problem, in *Handbook of Statistics* (Rao, C. R., Editor), 9: 377-408, Amsterdam: Elsevier Science Publishers.
9. Wendt F. 1933. Turbulente Stomungen Zwischen Zwei Rotierenden Konaxialen Zylindern, *Ingenieur Archiv*, 4: 577-595.

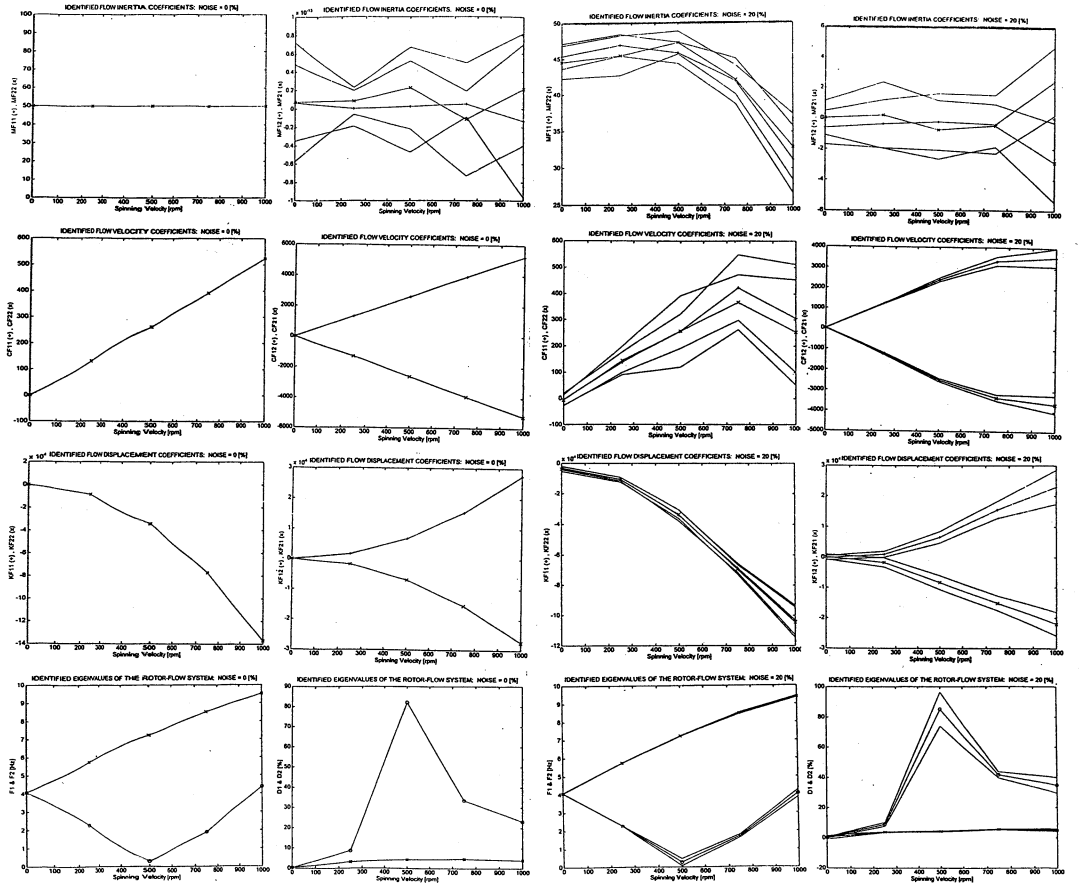

Figure 1. Numerical simulations test-case: Identification results using any time-domain method **(correlation** or **least-squares)**; Flow coupling coefficients and reconstructed modes as a function of Ω; Relative **noise contamination: 0 %** (10 averages , T_{block}=5 s).

Figure 2. Numerical simulations test-case: Identification results using the time-domain **correlation** or **ordinary least-squares** methods; Flow coupling coefficients and reconstructed modes as a function of Ω; Relative **noise contamination: 20 %** (10 averages , T_{block}=5 s).

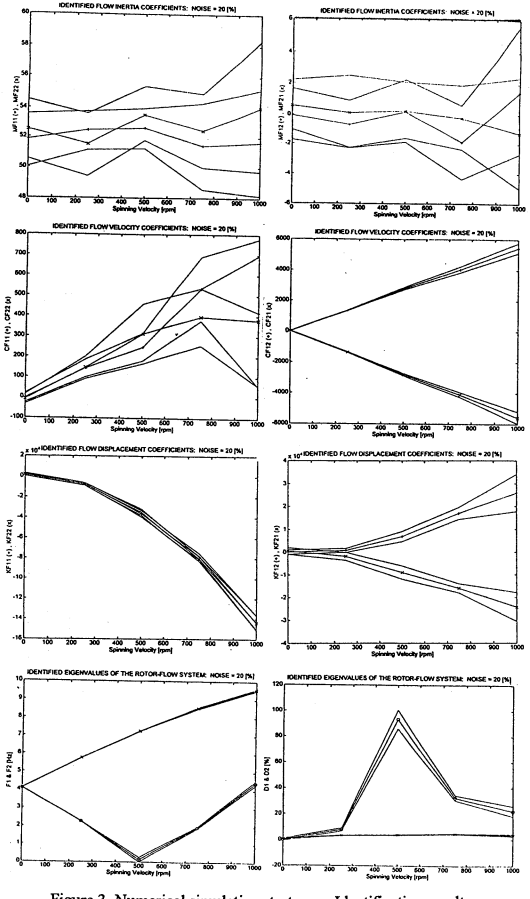

Figure 3. Numerical simulations test-case: Identification results using the time-domain **total least-squares** method; Flow coupling coefficients and reconstructed modes as a function of Ω; Relative **noise contamination: 20 %** (10 averages , T_{block}=5 s).

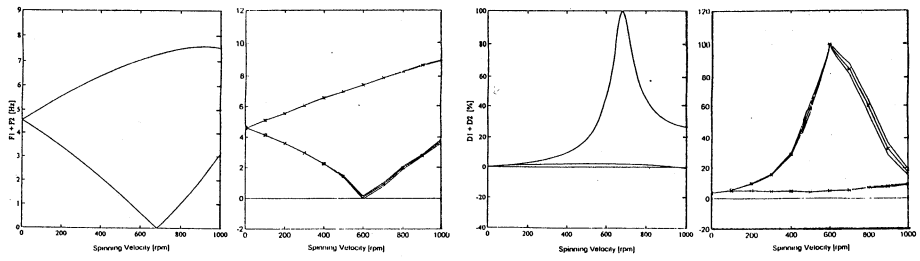

Figure 4. Results using the time-domain total **least-squares** method; Theoretical and identified modes as a function of Ω (10 averages , T_{block}=5 s).

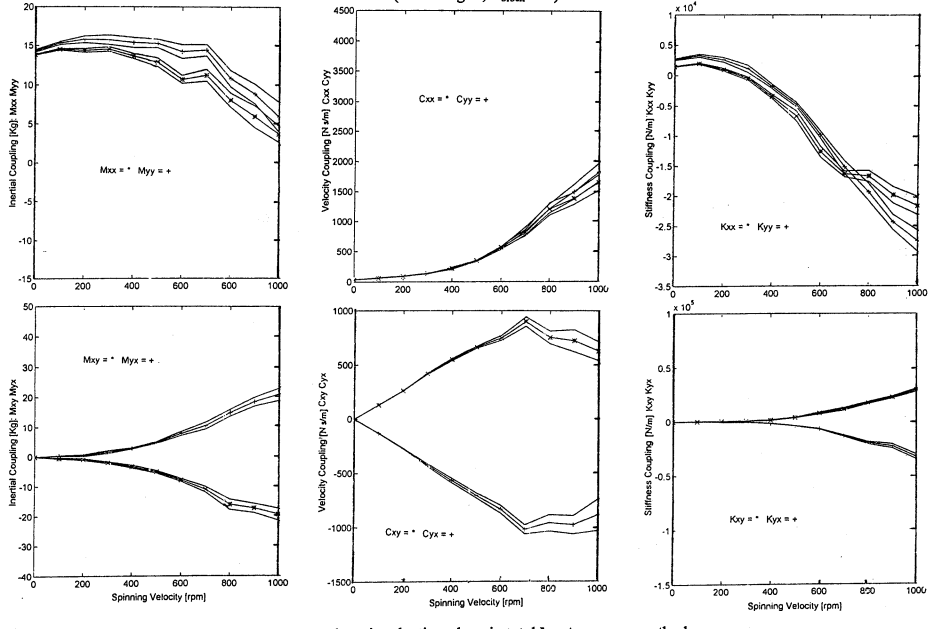

Figure 5. Results using the time-domain total **least-squares** method; Experimental flow-coupling coefficients as a function of Ω (10 averages , T_{block}=5 s).